Supporting Information

Zhang et al. 10.1073/pnas.1220253110

SI Methods

Protein Crystallization and Structure Determination. Details of protein expression, purification, and crystallization can be found in our previous reports (1, 2). Crystals of the protein complex (CaM + the channel fragment) were grown in either sitting or hanging drops by vapor diffusion at 20 °C (1, 3). The complex (1 mM) was mixed in a 1:1 ratio with the reservoir solution, which consisted of 1.25 M Li_2SO_4, 0.5 M $(NH_4)_2SO_4$, 0.1 M sodium citrate, pH 5.8. The diffraction data were processed using Xia2 (4). The crystallographic model was further constructed through iterative rounds of manual model building using Coot (5) and crystallographic refinement using REFMAC5 (6) and PHENIX (7). The NS309 structure was modeled in a hydrophobic pocket at the CaM-CaMBD interface at the CaM N-lobe based on strong electron density in difference Fourier maps and followed by successful refinement of the coordinates. Because of the poor water solubility of NS309, the protein complex was only 50% occupied by NS309. Due to the partial occupancy of NS309, portions of the structure were best modeled in two conformations, one corresponding to the NS309-bound structure, and the other to the NS309-free structure. A portion of an α-helix of the CaM N-lobe (residues 65 to 76) was modeled in two conformations. Consistent with NS309 partial occupancy, IDF residues 405–412 were modeled with 50% occupancy, and the density for this region was not as well resolved as the fully occupied regions of the structure. IDF residues H406 and M412 were truncated after the β-carbon due to disorder of the side chain, and in general IDF atoms have refined B-factors that are elevated relative to the rest of the structure. These features are expected since the IDF is an intrinsically disordered region of the structure. However, the side chain atoms of F410 are essentially the same as the overall average B-factor, consistent with their clear representation in electron density maps. Structure graphics were created using PyMol (Schrödinger, LLC).

Fluorescence Binding Assay. Binding assays were performed to investigate the Ca^{2+}-dependent interaction between CaM and CaMBD2-a, as previously described (1).

Electrophysiology. Details can be found in our previous papers (1, 2). The resistance of the patch electrodes ranged from 3–7 MΩ. EGTA (1 mM), DibromoBATA (0.1 mM), and HEDTA (1 mM) were mixed with Ca^{2+} to obtain desired free Ca^{2+} concentrations (http://www.stanford.edu/~cpatton/maxc.html). For Ca^{2+}-dependent channel activation, the current amplitudes at −90mV in response to various Ca^{2+} concentrations were normalized to that obtained at maximal Ca^{2+} concentration (10 μM). EC50s were determined by fitting the data points to a standard dose–response curve (Y = 100/[1 + (X/EC50)^-Hill)]. The dose response curves for NS309 were obtained at the Ca^{2+} concentration of 0.2 μM. MTS reagents were prepared as previously described (8). The MTS stock solution was diluted to its final concentration (2 mM) in bath solutions immediately before their application during experiments. The final concentration of MTS-1-MTS was 1 mM. Mutant cycle analyses were performed as previously described (9, 10). The coupling coefficient, Ω, is defined as Ω = {K(w:w) * K(m:m) / K(w:m) * K(m:w)}. W and M denote WT and mutants (CaM or SK2-a) respectively. When Ω is < 1, Ω = 1/Ω (9, 10). The standard deviation for Ω is calculated using the method of propagation of error.

1. Zhang M, et al. (2012) Structural basis for calmodulin as a dynamic calcium sensor. *Structure* 20(5):911–923.
2. Zhang M, Pascal JM, Schumann M, Armen RS, Zhang JF (2012) Identification of the functional binding pocket for compounds targeting small-conductance Ca2+-activated potassium channels. *Nat Commun* 3:1021.
3. Schumacher MA, Rivard AF, Bachinger HP, Adelman JP (2001) Structure of the gating domain of a Ca2+-activated K+ channel complexed with Ca2+/calmodulin. *Nature* 410(6832):1120–1124.
4. Winter G (2010) xia2: An expert system for macromolecular crystallography data reduction. *Journal of Applied Crystallography* 43(1):186–190.
5. Emsley P, Cowtan K (2004) Coot: Model-building tools for molecular graphics. *Acta Crystallogr D Biol Crystallogr* 60(Pt 12 Pt 1):2126–2132.
6. Collaborative Computational Project N (1994) The CCP4 suite: Programs for protein crystallography. *Acta Crystallogr D Biol Crystallogr* 50(Pt 5):760–763.
7. Adams PD, et al. (2010) PHENIX: A comprehensive Python-based system for macromolecular structure solution. *Acta Crystallogr D Biol Crystallogr* 66:213–221.
8. Yang N, George AL, Jr., Horn R (1996) Molecular basis of charge movement in voltage-gated sodium channels. *Neuron* 16(1):113–122.
9. Hidalgo P, MacKinnon R (1995) Revealing the architecture of a K+ channel pore through mutant cycles with a peptide inhibitor. *Science* 268:307–310.
10. Ranganathan R, Lewis JH, MacKinnon R (1996) Spatial localization of the K+ channel selectivity filter by mutant cycle based structure analysis. *Neuron* 16(1):131–139.

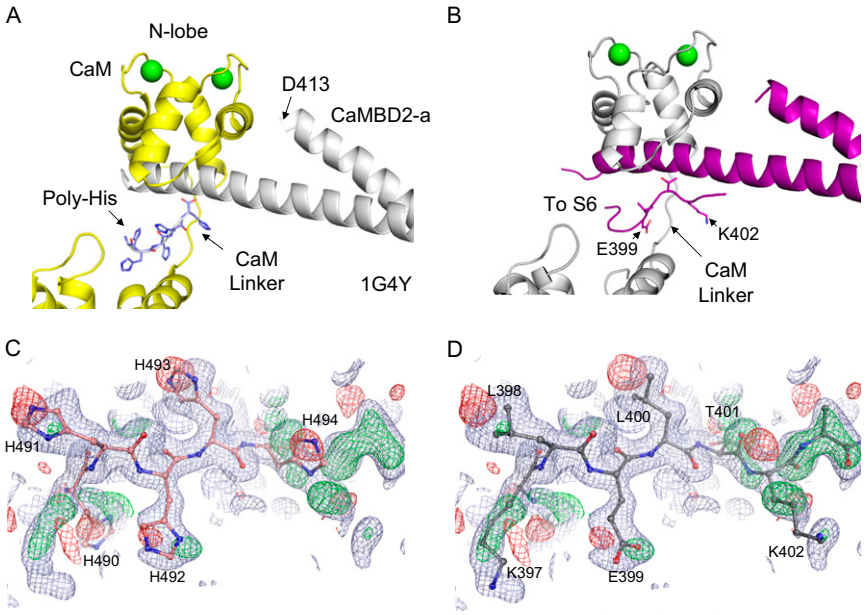

Fig. S1. The small-conductance Ca^{2+}-activated potassium channel KCa2.2 (SK2) fragment R396–M412 and its interaction with the calmodulin (CaM) linker. (*A*) Structure of 1G4Y, in which the CaM linker region was modeled to interact the polyhistidine (Poly-His) tag used to purify the CaM binding domain (CaMBD). Consequently, the entire fragment R396–M412 is missing in the structure of 1G4Y, even though it was part of the channel peptide used to obtain the protein crystals of the CaM–CaMBD complex. (*B*) A 1 × 1 structure model illustrating the location of the channel residues E399–K402. These four channel residues wrap around the CaM linker, forming a cuff-like structure. The model is rotated 180° along the *y* axis relative to the model in Fig. 1*B*. (*C*) 2Fo-Fc and Fo-Fc electron density maps were constructed using σA-weighted coefficients from REFMAC (1). The 2Fo-Fc map is drawn in light blue and contoured at 1.0 σ; the Fo-Fc map is contoured at +3.0 σ (green) and −3 σ (red). The maps were calculated using the CaM–CaMBD2-a diffraction data (Table S1) and a previous model, 1G4Y, in which histidine residues were modeled incorrectly in the cuff region. The Fo-Fc map shows strong peaks of negative difference density where histidine side chains have been modeled incorrectly and strong peaks of positive difference density where the previous model does not account for the entire cuff region. (*D*) The electron density maps shown in *C* but overlaid with our model for the cuff residues rather than with the polyhistidine model. Our model shows much better agreement with the electron density maps, even though the maps were constructed using the polyhistidine model to calculate phases.

1. Collaborative Computational Project, Number 4 (1994) The CCP4 suite: Programs for protein crystallography. *Acta Crystallogr D Biol Crystallogr* 50(Pt 5):760–763.

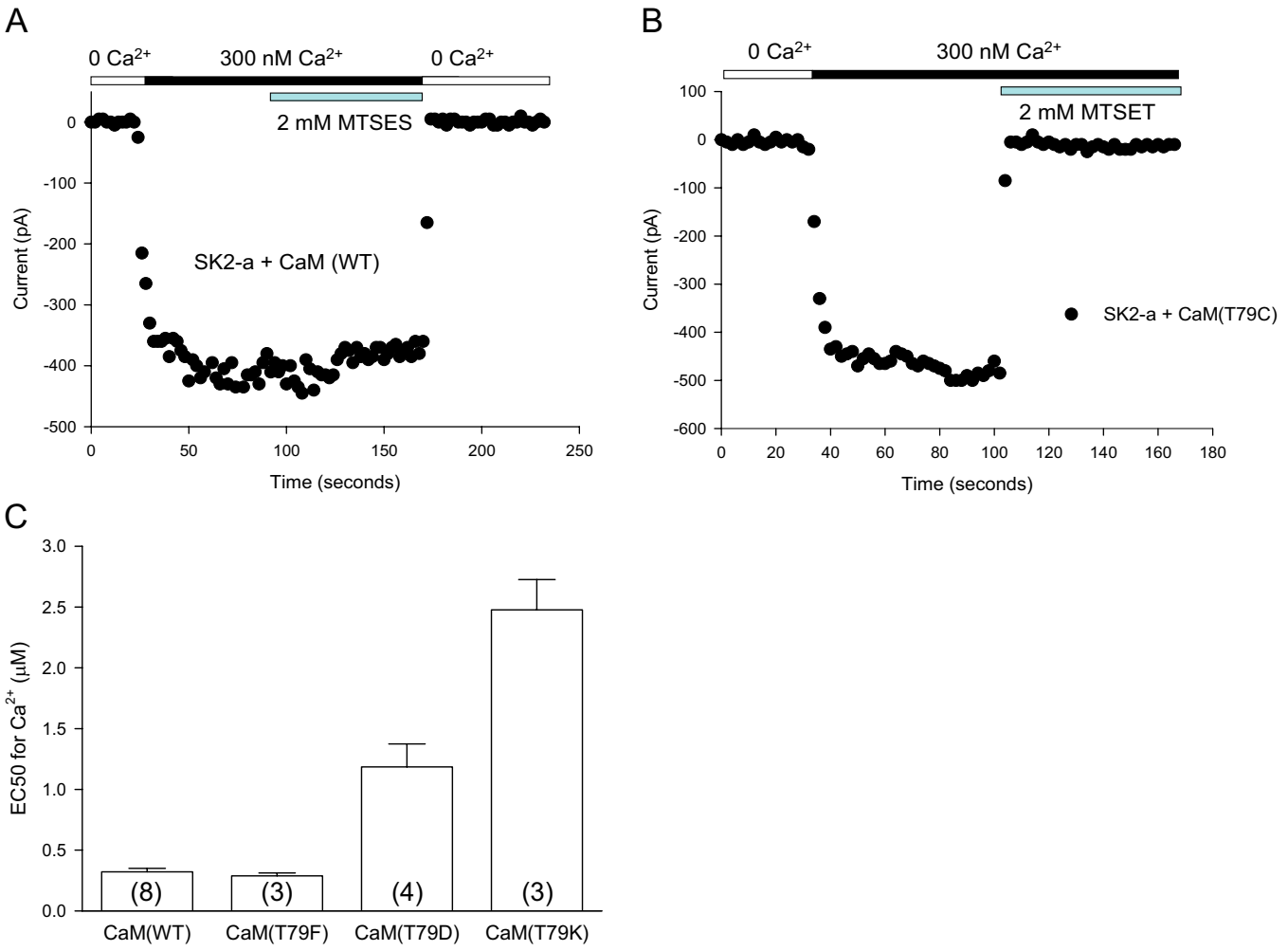

Fig. S2. Mutations of T79 of CaM and their effects on the Ca^{2+}-dependent activation of SK2-a channels (WT). (*A*) Application of 2-sulfonatoethyl methanethiosulfonate (MTSES, 2 mM) had no effect on SK2-a channels (WT). Although CaM does not have any cysteine residues, a total of nine cysteine residues are present in the SK2-a sequence. However, only one of the nine, C3, is located at the cytoplasmic side of the channel. (*B*) Effects of MTSET on T79C. The current amplitude is reduced quickly to zero upon application of 2-(trimethylammonium)ethyl methanethiosulfonate (MTSET, 2 mM). (*C*) The effects of charges at T79 are reproduced by mutant CaMs T79D and T79K when coexpressed with WT SK2a channels. T79F does not alter the Ca^{2+}-dependent activation of SK channels. Values in parentheses indicate the number of experiments.

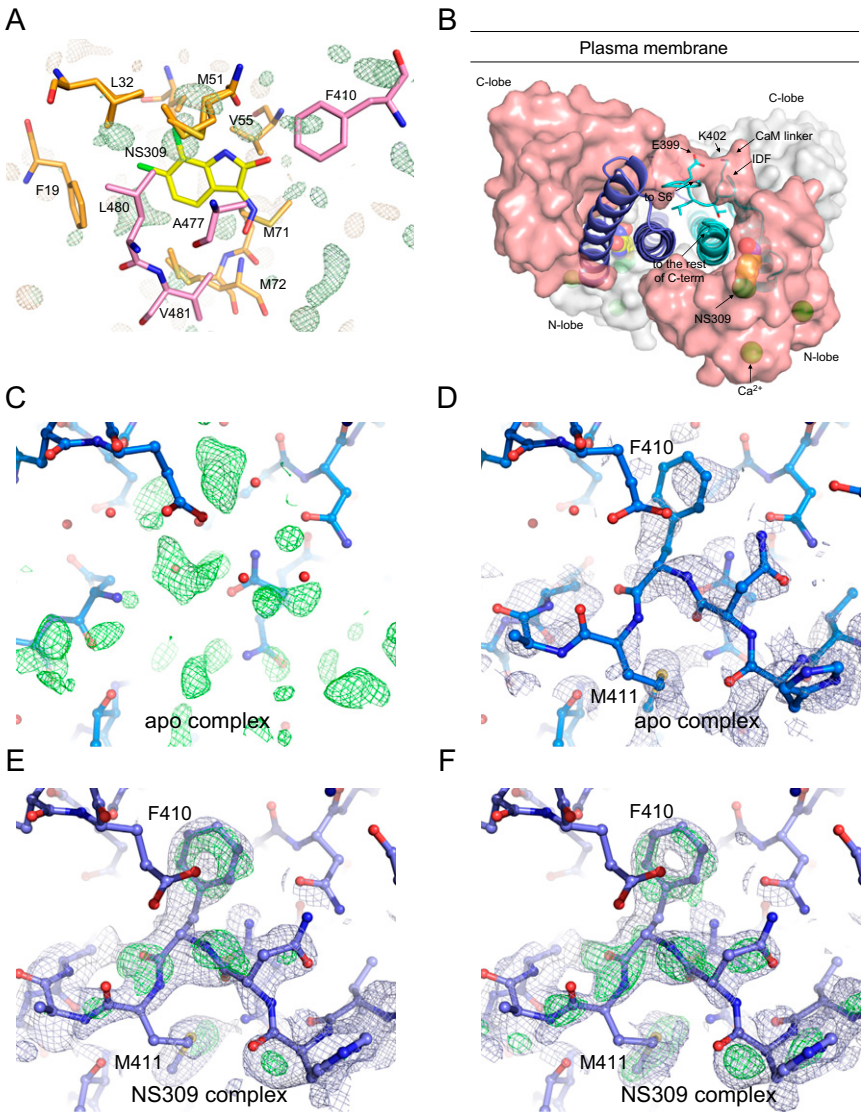

Fig. S3. Structure of the CaM–CaMBD2-a complex in the presence of NS309. (*A*) Difference Fourier electron density map constructed using mFo–DFc coefficients calculated in PHENIX before modeling the structure of the NS309-bound complex. The map is contoured at 3.0 σ and is overlaid with the final coordinates for NS309 (yellow), and residues from CaM (orange) and the CaMBD (pink) in the Ca^{2+}-bound CaM–CaMBD2-a complex. (*B*) Side view of the 2 × 2 complex shown in Fig. 3*C*. Both CaM molecules (salmon and gray) wrap around the two CaMBDs (blue and cyan) to form a 2 × 2 complex. Also shown are locations for NS309 and the appearance of the intrinsically disordered fragment (IDF). The CaM complex is located very close to the plasma membrane because of the interaction between the channel cuff and the CaM linker. (*C*) Fo-Fc difference electron density map in the region of the IDF for the CaM–CaMBD complex determined in the absence of bound ligand (apo complex). The map is contoured at 2.0 σ and shows only spurious peaks of positive density. (*D*) The IDF was added to the model for the apo CaM–CaMBD complex, and the resulting model was refined against the diffraction data. The IDF is not well represented in the resulting 2Fo-Fc electron density map (in blue, 0.6 σ), indicating that this region is not well ordered in the apo CaM–CaMBD complex. (*E*) Electron density maps calculated in the region of the IDF for the CaM–CaMBD/NS309 complex. The Fo-Fc map was calculated before the modeling of the IDF (in green, contoured at 2.0 σ). The density difference in this map and iterative model building allowed us to construct a model for the IDF. A 2Fo-Fc map was calculated for the final model that includes the IDF (in blue, contoured at 0.6 sigma). (*F*) IDF residues 402–412 were removed from the CaM–CaMBD/NS309 model, and the coordinates were refined against the diffraction data using a simulated annealing protocol in PHENIX (1). The resulting 2Fo-Fc map (blue, 0.6 σ) and Fo-Fc map (green, 2.8 σ) demonstrate positive peaks of electron density for the IDF, even though it was not included in the model during refinement, thus confirming the model for the IDF.

1. Adams PD, et al. (2010) PHENIX: A comprehensive Python-based system for macromolecular structure solution. *Acta Crystallogr D Biol Crystallogr* 66(Pt 2):213–221.

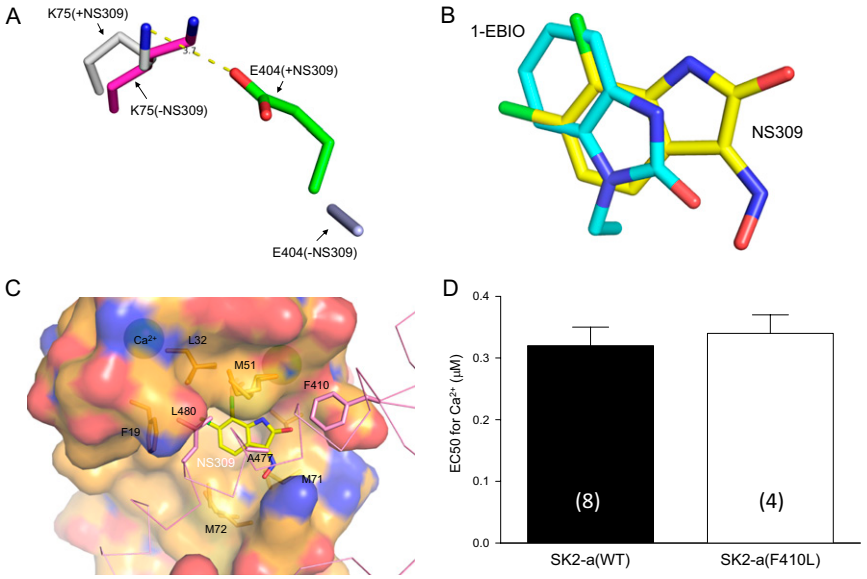

Fig. S4. Unique features of the NS309-bound structure. (*A*) Formation of a salt bridge between K75 of CaM (gray) and E404 of the IDF (green) in the presence of NS309. Without NS309, the conformation of E404 (light blue) cannot be determined beyond the β-carbon. The distance between K75 and E404 is 3.7 Å in the presence of NS309. (*B*) The binding site for NS309 overlaps with that of 1-EBIO. Shown are the structures of NS309 (yellow) and 1-EBIO (cyan) in their respective protein complexes. 1-EBIO is much less potent than NS309 in potentiating the SK channel activity. (*C*) Amino acid residues involved in formation of the NS309 binding pocket. Shown are the key amino acid residues that form the NS309 binding site, including F410, A477, and L480 from the channel and F19, L32, M51, M71, and M72 of CaM (within the radius of 5 Å). Because NS309 has poor water solubility, the occupancy of the binding site by NS309 is not 100%. Therefore some of the amino acid residues are modeled in two different conformations, one representing the NS309-bound conformation and the other the NS309-free conformation. For instance, M51 and M72 are shown both conformations, but M71 is shown its NS309-bound conformation. Unlike NS309, 1-EBIO does not interact directly with F410. (*D*) F410L mutation does not change the Ca^{2+}-dependent activation of the mutant channel. Values in parentheses indicate the number of experiments.

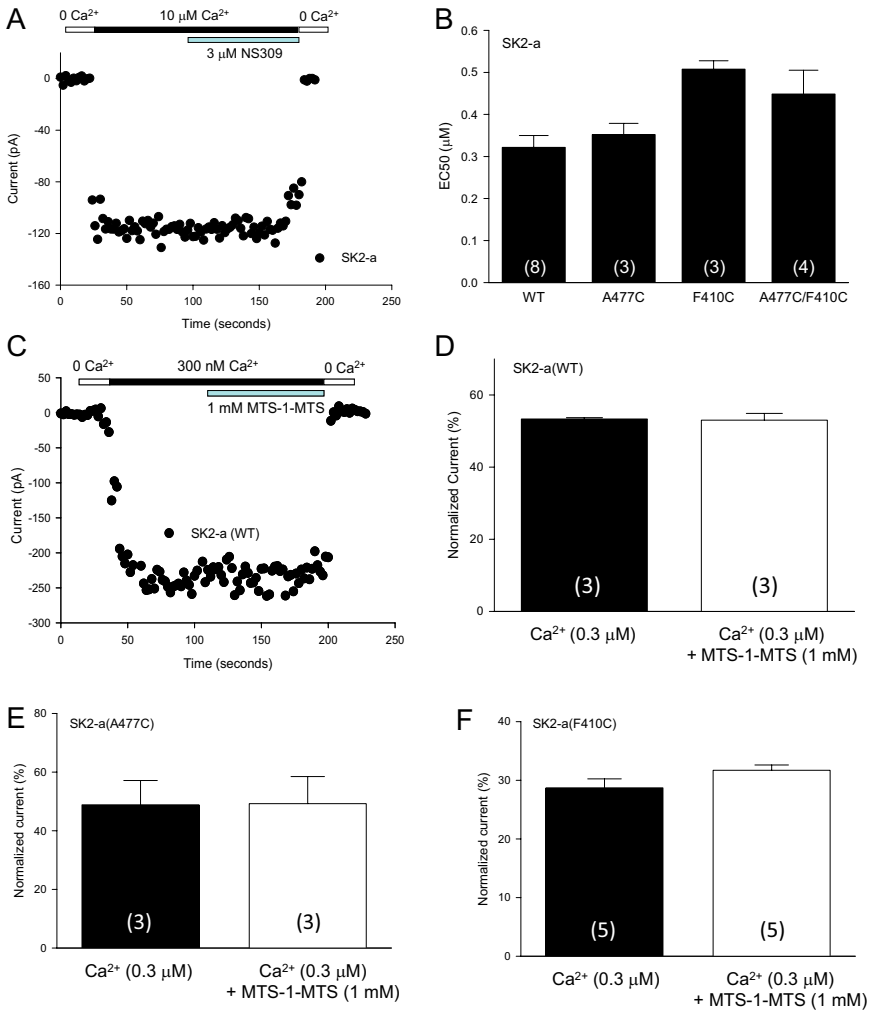

Fig. S5. NS309 on SK channels and cross-linking of A477C of the CaMBD and F410C of the IDF by MST-1-MST. (*A*) NS309 has no additional effects on SK channel activity when the SK channel activation has reached its maximum at 10 μM Ca^{2+}. (*B*) A double mutant, A477C/F410C, becomes less sensitive to Ca^{2+} for its activation with a slight increase in EC_{50}. The increase, however, is caused by F410C, not by A477C. The EC_{50}s are 0.32 ± 0.03 μM, 0.35 ± 0.03 μM, 0.51 ± 0.02 μM, and 0.45 ± 0.06 μM for WT, A477C, F410C, and A477C/F410C, respectively. Values in parentheses indicate the number of experiments. (*C* and *D*) Methanediyl bismethanethiosulfonate (MTS-1-MTS, 1 mM) has no effects on Ca^{2+}-dependent channel activation of WT SK2-a channels (53.33 ± 0.38% vs. 53.01 ± 1.87%, $n = 3$). (*E* and *F*) MTS-1-MTS (1 mM) has little effect on the single cysteine mutation A477C (48.83 ± 8.31% vs. 49.22 ± 9.25%, $n = 3$) or F410C (28.43 ± 1.80% vs. 30.96 ± 1.66%, $n = 5$).

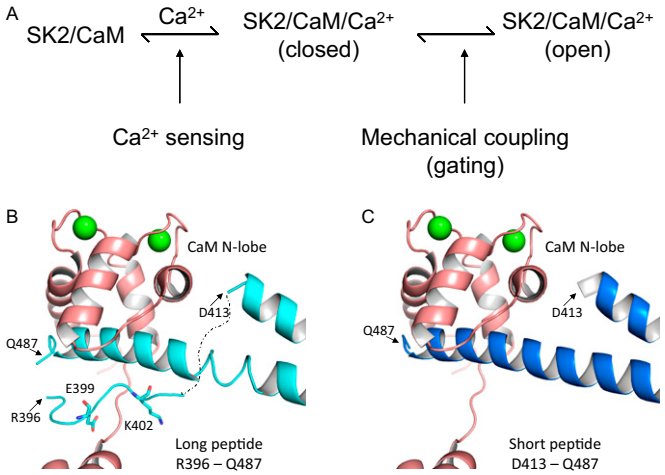

Fig. S6. A simple gating scheme for activation of SK channels by Ca^{2+}. (*A*) At least two steps are required for (*i*) binding of Ca^{2+} to CaM and (*ii*) transition of the CaM/Ca^{2+}-bound SK channel from the closed state to the open state. Changes at either step may appear as a shift of Ca^{2+} dose–response curves for channel activation. (*B* and *C*) Structures of the CaM–CaMBD2-a complex with (*B*) or without (*C*) the channel fragment R396–M412. Fluorescence-based binding assays were performed using two different SK2 channel peptides, a longer one (R396–Q487) and a shorter one (D413–Q487), and CaM to measure the apparent K_d for Ca^{2+} in formation of the CaM–CaMBD2-a complex. The long peptide includes the cuff, intrinsically disordered protein, and the CaMBD, whereas the short one has the CaMBD only.

Table S1. Crystallographic statistics

	CaM–CaMBD2-a	CaM–CaMBD2-a with NS309
Data collection*		
Space group	C2	C2
Unit cell (Å)	$a = 77.6$, $b = 66.8$, $c = 64.8$	$a = 77.2$, $b = 66.9$, $c = 64.8$
Dimensions (°)	$\alpha = 90.0$, $\beta = 94.5$, $\gamma = 90.0$	$\alpha = 90.0$, $\beta = 9\ 3.8$, $\gamma = 90.0$
Wavelength (Å)	1.12	1.08
Resolution range (Å)	40–1.51 (1.55–1.51)	30–1.66 (1.70–1.66)
Completeness (%)	96.3 (94.0)	99.6 (99.7)
Total observations	261,337 (19,146)	202,021 (14,822)
Unique observations	49,769 (3,595)	38,789 (2,884)
Mean redundancy	5.3 (5.3)	5.2 (5.1)
Mean I/σ(I)	24.1 (2.7)	17.7 (2.5)
R_{merge} †	0.035 (0.682)	0.052 (0.733)
R_{pim} ‡	0.017 (0.326)	0.025 (0.357)
Model refinement*		
Resolution range (Å)	40–1.51 (1.54–1.51)	30–1.66 (1.70–1.66)
No. reflections	49,765 (2,502)	38,789 (2,771)
R_{work} §	0.173 (0.265)	0.192 (0.262)
R_{free} §	0.206 (0.295)	0.225 (0.318)
No. atoms/average B (Å^2)	2,456/30.3	2,277/36.4
Protein	2,104/28.8	2,079/35.8
Calcium ions	2/29.8	2/38.7
Solvent	208/39.1	182/44.2
Ligand	0	14/39.4
Phi/Psi angles favored (%)/no. outliers	98.7/0	97.7/0
rmsd bond angles (°)	1.260	1.126
rmsd bond lengths (Å)	0.010	0.0075

*Values in parentheses refer to data in the highest-resolution shell.

†$R_{merge} = \sum_{hkl}\sum_j |I_j - \langle I\rangle| / \sum_{hkl}\sum_j I_j$. $\langle I\rangle$ is the mean intensity of j observations of reflection *hkl* (Miller indices) and its symmetry equivalents.

‡$R_{pim}\,(\text{precision} - \text{indicating merge}) = \sum_{hkl}(1/n_{hkl} - 1)^{1/2}\sum_j |I_j - \langle I\rangle| / \sum_{hkl}\sum_j I_j$. n is the number of observations of reflection *hkl*.

§$R_{cryst} = \sum_{hkl} |F_{obs} - kF_{calc}| / \sum_{hkl} F_{obs}|$. $R_{free} = R_{cryst}$ for 5% of reflections excluded from crystallographic refinement.